


ORIGINAL RESEARCH

Open Access



Reduced sulfur compounds and carboxylic acid groups in dissolved PFRs of iron-biochar enhance Cr(VI) reduction in anaerobic conditions

Shujie Hu^{1,3}, Chengshuai Liu^{2*} , Hongling Bu⁴, Manjia Chen¹, Jiao Tang⁵, Bin Jiang⁵ and Yong Ran⁵

Abstract

In addition to the adsorption and immobilization capacities of iron-modified biochars, these materials produce persistent free radicals (PFRs) that can carry out metal [i.e., Cr(VI)] redox transformations, but the primary forms and active species of PFRs involved are not well understood. Here, we investigated the key species of PFRs of α -Fe₂O₃-modified biochar (MBC) and their influence on Cr(VI) reduction under anaerobic conditions simulating paddy soil environments. MBC produced bulk phenoxyl PFRs that promoted Cr(VI) reduction due to the catalytic effect of the transition metal Fe. In addition, MBC was more efficient in reducing Cr(VI) under anaerobic conditions than under aerobic conditions due to the more active and accessible dissolved PFRs present in the dissolved organic matter (DOM). The electron transfer capacity of DOM was demonstrated by excitation-emission matrix (EEM) spectrophotometry combined with parallel factor analysis, which showed that the protein-like and humic-like components of DOM were involved in Cr(VI) reduction. Furthermore, Fourier transform ion cyclotron resonance mass spectrometry (FTICR-MS) analysis indicated that reduced-S compounds (O/S < 4) and carboxylic acid (–COO) groups in the unsaturated aliphatic and lignin-like compounds are potentially the main active species accelerating Cr(VI) reduction under anaerobic conditions. Our results provide new insights into the role of dissolved PFRs from iron-modified biochar in promoting Cr(VI) reduction under anaerobic conditions such as flooded soils.

Highlights

- Iron modification promoted a 5.6-fold increase in the concentration of bulk phenoxyl PFRs over unmodified biochar.
- Dissolved PFRs in iron-biochar derived dissolved organic matter enhanced Cr(VI) reduction under anaerobic conditions.
- Reduced sulfur compounds and carboxylic acid groups were the major reducing species in the dissolved PFRs.

Keywords Biochar, Iron-modification, PFRs, Hexavalent chromium, Anaerobic condition

Handling editor: Bin Gao.

*Correspondence:

Chengshuai Liu

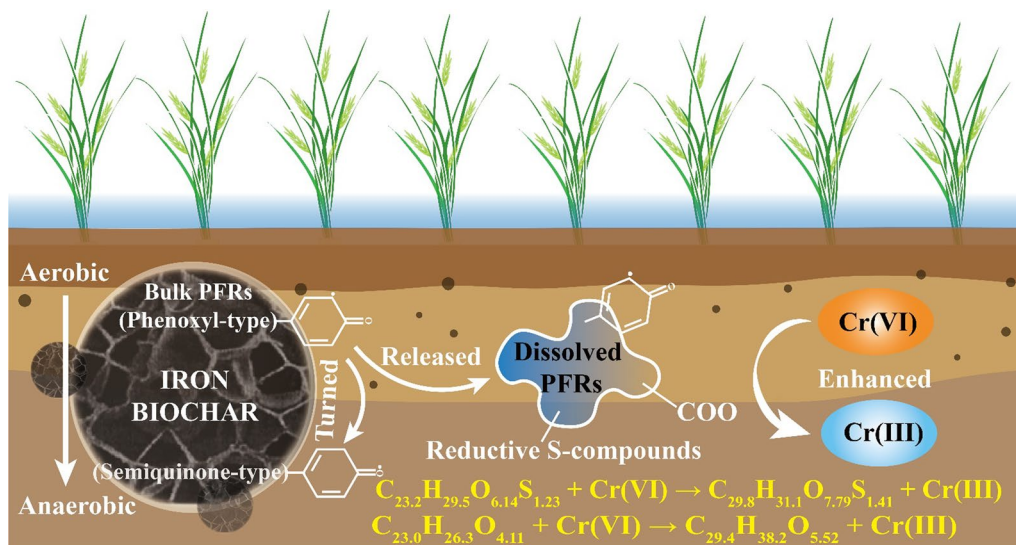
liuchengshuai@vip.gyig.ac.cn

Full list of author information is available at the end of the article



© The Author(s) 2024. **Open Access** This article is licensed under a Creative Commons Attribution 4.0 International License, which permits use, sharing, adaptation, distribution and reproduction in any medium or format, as long as you give appropriate credit to the original author(s) and the source, provide a link to the Creative Commons licence, and indicate if changes were made. The images or other third party material in this article are included in the article's Creative Commons licence, unless indicated otherwise in a credit line to the material. If material is not included in the article's Creative Commons licence and your intended use is not permitted by statutory regulation or exceeds the permitted use, you will need to obtain permission directly from the copyright holder. To view a copy of this licence, visit <http://creativecommons.org/licenses/by/4.0/>.

Graphical Abstract



1 Introduction

Biochar, due to its redox activity in contaminant removal in water and soil systems, has attracted considerable interest (Fei et al. 2022; Zhu et al. 2020; Yuan et al. 2017; Klüpfel et al. 2014). Through its electron transfer and mediation capabilities, biochar can facilitate the degradation and transformation of environmental contaminants, thereby influencing their biogeochemical cycling and environmental fate (Yuan et al. 2017; Klüpfel et al. 2014). Generally, phenolic moieties and conjugated π -electrons in biochar, as well as persistent free radicals (PFRs) on biochar, contribute to its electron transfer capability (Cuong et al. 2021; Klüpfel et al. 2014).

PFRs, as a class of organic free radicals on biochar, have great potential for applications in micropollutant transformation in the environment (Fang et al. 2014, 2015; Zhu et al. 2020). PFRs can trigger sequential single-electron transfer to oxidants (i.e., H_2O_2 and O_2) to generate reactive oxygen species (ROS, $\cdot\text{OH}$, $\cdot\text{O}_2^-$, etc.) for the degradation of organic pollutants (Fang et al. 2014, 2015). The direct reductive capacity of PFRs has also been demonstrated for *p*-nitrophenol degradation and Cr(VI) remediation (Zhu et al. 2020; Yang et al. 2016a). For example, PFRs on biochar can reduce Cr(VI) to less toxic Cr(III) through direct single-electron transfer and indirect formation of $\cdot\text{O}_2^-$ (Xu et al. 2020a; Zhu et al. 2020). Our recent study showed that PFRs on iron-modified biochar can promote Fe(III)/Fe(II) cycling and accelerate the reduction of Cr(VI) to Cr(III) (Hu et al. 2024). The transformation reactions of PFRs to contaminants

in these studies were predominantly executed under aerobic conditions. The reactivity of PFRs under anaerobic environments, such as inundated paddy soil, is rarely reported (Fang et al. 2014, 2015; Xu et al. 2020a; Zhu et al. 2020). To date, only two recent studies have focused on the reactivity of PFRs under anaerobic conditions (Guan et al. 2023; Xu et al. 2023). Based on solution color development after a reaction, Guan et al. (2023) reported that biochar-based PFRs could react with tertiary butanol under anaerobic conditions, but no relevant mechanism was investigated. Xu et al. (2023) revealed that PFRs could transfer electrons to H_2O to form $\cdot\text{O}_2^-$, which promoted the abiotic oxidation of tire antioxidants. Therefore, further investigations are needed on the reaction mechanisms of PFRs under anaerobic environments. Anaerobic environments are more prevalent in deep soils or flooded paddy soils, which are commonly contaminated with hexavalent Cr(VI) near urban industrial areas, threatening the safety of agricultural products and human health (Liu et al. 2021). However, the mechanism of Cr(VI) reduction by biochar PFRs under anaerobic conditions is not clear.

Dissolved organic matter (DOM) also contains these “long-lived” PFRs (Jacobs et al. 2012), and the reactivity of PFRs is higher in biochar-derived DOM than in bulk biochar (Chen et al. 2021; Dong et al. 2014; Lian et al. 2020). The PFRs present in DOM can increase the number of contact sites with pollutants (Lian et al. 2020). Here, these PFRs in the DOM are considered to be dissolved PFRs. In addition, lignin in river water DOM

and saturated compounds in soil DOM were the main species promoting sulfamethoxazole degradation and arsenic oxidation under aerobic conditions, as determined by Fourier transform ion cyclotron resonance mass spectrometry (FTICR-MS) (Liang et al. 2023; Zeng et al. 2021). In our previous investigation, we focused exclusively on the bulk PFRs in biochar (Hu et al. 2024). However, the key active compounds of DOM for Cr(VI) reduction under anaerobic conditions, especially the essential reductive species in biochar-derived dissolved PFRs, remain undetermined. A combination of excitation-emission matrix (EEM) spectroscopy and ultrahigh-resolution FTICR-MS (Jia et al. 2021; Zeng et al. 2021) could allow the identification of key dissolved PFRs active species involved in Cr(VI) reduction and thus improve our understanding of the redox processes occurring in dissolved PFRs under anaerobic soil conditions.

Therefore, in this study, iron oxide (α -Fe₂O₃) modified rice husk biochar with high PFRs contents was prepared to investigate the reactivity and major active species of biochar-derived PFRs under anaerobic conditions. This research can help to provide a new perspective on the reductive species released by iron-biochar, and improve the understanding of the molecular reduction mechanism of Cr(VI) by iron-biochar.

2 Materials and methods

2.1 Preparation of biochar and iron-biochar

Rice husk was selected as the biomass. Since in our prior study, it was reported that the content of PFRs was highest for biochar prepared at a 500 °C pyrolysis temperature (Hu et al. 2024), the subsequent iron-modified biochar was synthesized at 500 °C. Nanometer-sized α -Fe₂O₃ powder was mixed with rice husk (Fe/biomass = 5%, w/w) by using a Pulverisette-6 Planetary Mill (FRITSCH, Germany) for 1 h. The mixed sample was slowly pyrolyzed at 500 °C in a tube furnace (GSL-1100-X, HF-Kejing, China) under a N₂ atmosphere for 2 h, yielding MBC. Biochar without added α -Fe₂O₃ was included as a control sample and designated BC.

2.2 Characterization of biochar and iron-biochar

The C, H, O, N, and S contents, pH, zeta potential, microporosity, surface morphologies, surface elemental compositions (C, O, S, Fe, and Cr), oxygen functional groups, and crystalline iron in BC and MBC were determined as reported in our previous study (Hu et al. 2024) and can be referred to in Additional file 1: Text S1. The dissolved sulfate in biochar was extracted with deionized water (1:20 w/v) for 1 h, and sulfate concentrations were determined by ion chromatography (ICS-5000+, Thermo Fisher Scientific, USA).

2.3 Batch sorption kinetics and isothermal sorption experiments

Anaerobic Cr(VI) sorption kinetic and isothermal sorption experiments were conducted with MBC and BC in a glovebox filled with 3–5% H₂-balanced N₂. The Cr(VI) solution was first purged with high purity N₂ (99.999%) for 2 h to remove dissolved oxygen. The biochar samples were placed in a glovebox for 2 days prior to the experiment for removal of adsorbed O₂. Batch Cr(VI) sorption by MBC and BC was performed as described in our previous study (Hu et al. 2024). All sorption experiments were conducted in triplicate. Briefly, 2.0 g of the biochar sample was added to 200 mL of 50 mg L⁻¹ Cr(VI) solution in a 250 mL glass bottle. The pH was adjusted to 3.0 ± 0.1 with the addition of 0.1 M HCl or NaOH solution. No buffer was added for this experiment. Kinetic experiments were performed in the dark at 25 ± 1 °C and 500 rpm. Samples were collected from the solution at different reaction times (0, 0.5, 1, 2, 3, 4, 8, 12, and 24 h) and then filtered through a 0.45 µm membrane (PTFE). At the end of the kinetic experiments, biochar particles were collected, rinsed with deionized water, and freeze-dried prior to X-ray photoelectron spectroscopy (XPS) and electron paramagnetic resonance (EPR) analysis. For subsequent DOM analysis, the filtered solution was collected. Concentrations of total Cr, Cr(VI), Cr(III), total Fe, Fe(II), and Fe(III) in solution were measured and are detailed in Additional file 1: Text S2. Sorption kinetic models of pseudo-first-order (PFO) and pseudo-second-order (PSO) are provided in Additional file 1: Text S3.

For isothermal sorption experiments, Cr(VI) solutions ranged from 5 to 1000 mg L⁻¹. Cr(VI) solution and biochar were mixed at a ratio of 100:1 in 15 mL centrifuge tubes. Centrifuge tubes were shaken in the dark at 25 ± 1 °C and 250 rpm for 48 h. Total Cr, Cr(VI), total Fe, and Fe(II) concentrations in solution were then determined. Sorption isotherm models of Freundlich and Langmuir are listed in Additional file 1: Text S3. The experiments for aerobic Cr(VI) sorption kinetics and isothermal sorption by MBC and BC were carried out under conditions without oxygen controlling, and the other sorption conditions were consistent with anaerobic experiments.

2.4 EPR and quenching experiments

To quantify the intensity of bulk PFRs, 20 mg of BC or MBC was injected into a micropipette in an EPR instrument (Bruker A300 spectrometer, Germany). The specific parameters were as follows: center field 3510 G, sweep width 300 G, microwave frequency 9.85 GHz, microwave power 19.23 mW, modulation frequency 100 kHz, modulation amplitude 1.0 G, and sweep time 60.42 s (Liang

et al. 2020; Zhu et al. 2020). As the dissolved PFRs cannot be isolated from DOM, we characterized the DOM in this study instead of the dissolved PFRs. DOM was collected through a 0.45 μm pre-combusted glass fiber filter membrane (Whatman), freeze-dried, and measured by EPR in subsequent kinetic experiments.

ROS identification was performed using EPR coupled with 5,5-dimethyl-1-pyrroline-*N*-oxide (DMPO) as a spin-trapping agent to characterize $\cdot\text{O}_2^-$ and $\cdot\text{OH}$ (Han et al. 2022). 4-Amino-2,2,6,6-tetramethylpiperidine (TEPM) was used to capture $^1\text{O}_2$. Briefly, each 10 g L^{-1} biochar suspension was filtered after 10 min or 30 min dark shock. The filtered solution was then mixed with 100 mM scavenger in a 1:1 volume ratio to obtain 1 mL of mixed solution. Then, 30 μL of the mixed solution was absorbed into a capillary glass tube for the EPR assay.

Moreover, to identify the impacts of ROS on Cr(VI) reduction, different scavengers were used as electron competitors during the quenching tests. ρ -Benzoquinone (BQ, 100 mM) was added to probe $\cdot\text{O}_2^-$, isopropanol (IPA, 100 mM) and terephthalic acid (TPA, 50 μM) were used to probe $\cdot\text{OH}$, and furfuryl alcohol (FFA, 100 mM) was selected to act as the scavenger of $^1\text{O}_2$ (Zhu et al. 2020, 2022; Liu et al. 2022).

2.5 UV-vis absorption spectra and EEM fluorescence spectra

Absorption and fluorescence spectra of biochar-derived DOM before and after Cr(VI) removal were obtained simultaneously using an Aqualog fluorometer (HORIBA Scientific, USA). The detailed UV-vis and fluorescence properties are listed in Additional file 1: Text S4. A total of 40 EEMs from MBC and BC were corrected and decomposed using parallel factor analysis (PARAFAC) to extract components using the drEEM toolbox version 2.0 with MATLAB software (<http://models.life.ku.dk/drEEM>, last accessed: June 2014) (Murphy et al. 2013), and the details were described in our previous studies (Tang et al. 2020, 2021). A two- to seven-component PARAFAC model was explored in the context of core consistency and residual analysis (Additional file 1: Figs. S1 and S2). A four-component PARAFAC model was identified, which explained 95.8% of the variance and successfully passed the split-half validation test with a split style of $\text{S}_4\text{C}_6\text{T}_3$ (Additional file 1: Fig. S3), indicating that the model was stable.

2.6 Ultrahigh-resolution electrospray ionization FTICR-MS analysis

Eight DOM samples of MBC and BC were selected for FTICR-MS analysis. These samples were taken before and after 24 h of reaction with Cr(VI) under anaerobic and aerobic conditions. Desalting and concentration of anaerobic DOM were performed, and the samples were

kept in a glovebox to prevent O_2 exposure until FTICR-MS analysis. The DOM samples were desalted and concentrated using Varian Bond Elute PPL cartridges (1 g per 6 mL) (Lv et al. 2016; Spencer et al. 2014; Dittmar et al. 2008). Our previous study showed that the average extraction efficiency for DOM routinely obtained with this procedure yielded an average value of 71.8% (on a carbon basis, unpublished data). Ultrahigh-resolution mass spectra for the purified DOM fractions were acquired using a solaris X XR FTICR-MS (Bruker Daltonik GmbH, Bremen, Germany) equipped with a 9.4 T refrigerated actively shielded superconducting magnet (Bruker Biospin, Wissembourg, France) and a Paracell analyzer cell. Samples were ionized by electrospray ionization (ESI) (Bruker Daltonik GmbH, Bremen, Germany) in negative ion mode. The detection mass range was set to m/z 100–800. Elemental ratios of $\text{O}/\text{C} \leq 1.2$ and $\text{H}/\text{C} \leq 2.5$ were used to further constrain the formula calculations. The O/C ratio, H/C ratio, molecular weight (MW), nominal oxidation state of carbon (NOSC), double bond equivalent (DBE), and modified aromaticity index (AI_{mod}) were used to describe the molecular properties of DOM, which are detailed in Additional file 1: Text S5. Seven molecular groups were further delineated by the AI_{mod} and H/C cutoffs (Lv et al. 2016; Spencer et al. 2014): (1) saturated compounds ($\text{H}/\text{C} > 2$), (2) peptides ($2 > \text{H}/\text{C} \geq 1.5$ and $\text{N} > 0$), (3) unsaturated aliphatic compounds ($2 > \text{H}/\text{C} \geq 1.5$ and $\text{N} = 0$), (4) carbohydrates ($\text{H}/\text{C} \leq 2$, $\text{O}/\text{C} > 0.9$), (5) lignin-like/phenolic formulas ($\text{AI}_{\text{mod}} \leq 0.5$ and $\text{H}/\text{C} < 1.5$), (6) aromatic formulas ($0.5 < \text{AI}_{\text{mod}} \leq 0.66$), and (7) condensed aromatic formulas ($\text{AI}_{\text{mod}} > 0.66$).

3 Results and discussion

3.1 Cr(VI) removal and transformation

Iron modification significantly improved the conversation of Cr(VI). The amount of Cr(VI) removed and the amount of Cr(III) generated by MBC were 1.69–1.76 and 1.49–3.18 times higher than those by BC, respectively (Fig. 1a, b and Additional file 1: Fig. S4a, b). The amount of Cr(VI) removed by MBC was 48.6 mg L^{-1} within 24 h under anaerobic conditions, much higher than the 34.8 mg L^{-1} of Cr(VI) removed under aerobic conditions (Fig. 1a). The models for the kinetics of Cr(VI) removal and sorption isotherms showed higher values under anaerobic conditions compared to aerobic conditions (Additional file 1: Tables S1 and S2). Further discussion can be found in Additional file 1: Text S6. However, the amount of Cr(III) produced by MBC was lower under anaerobic conditions (0.72–2.78 mg L^{-1}) than under aerobic conditions (1.31–7.77 mg L^{-1}) (Fig. 1b). These results suggest that O_2 has a dual effect on Cr(VI) removal and Cr(III) generation by MBC. Cr(VI) is more

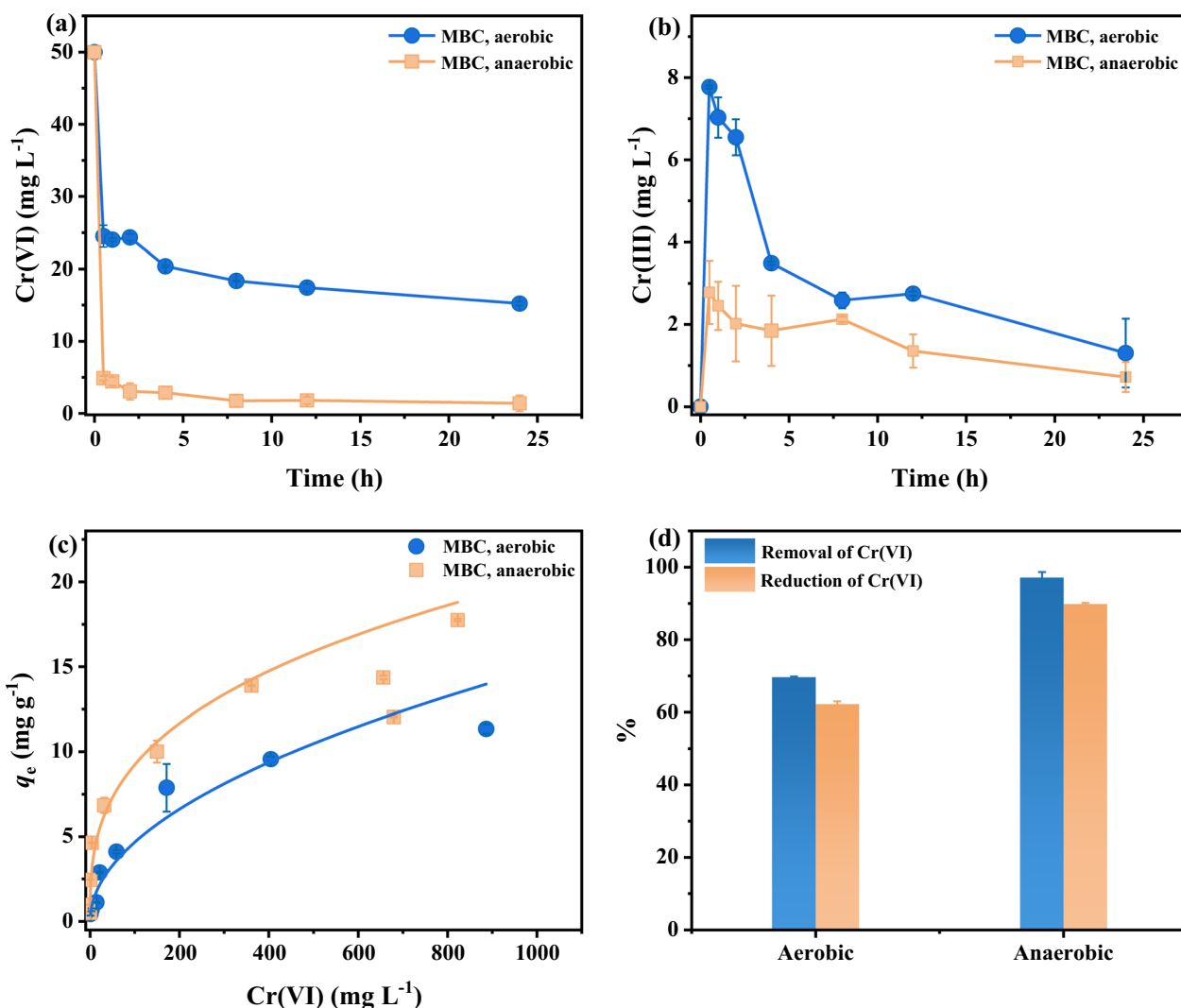


Fig. 1 a Cr(VI) removal kinetics; b Cr(III) generation kinetics; c Cr(VI) adsorption isotherms; and d Cr(VI) removal and reduction efficiencies of MBC

efficiently removed under anaerobic conditions, while Cr(III) is predominantly formed under aerobic conditions. This disparity is due to an electron transfer mechanism under aerobic conditions where electrons from PFRs are transferred to O₂, producing ·O₂⁻ which facilitates Cr(VI) reduction, resulting in a higher concentration of Cr(III). Conversely, aerobic environments harbor an abundance of ROS (such as ·OH and ¹O₂) with higher redox potentials that have the ability to re-oxidize the reduced Cr(III), resulting in a diminished Cr(VI) removal efficiency compared to anaerobic conditions (a detailed discussion is provided in the subsequent section). In addition, the concentrations of Cr(III) for MBC initially increased rapidly and then decreased with increasing reaction time due to the electrostatic attraction between MBC and Cr(III) (Fig. 1b and Additional file 1: Figs. S5a and S6). However, the decreases in the concentrations of

Cr(III) were much greater under aerobic conditions than under anaerobic conditions (Fig. 1b), suggesting the re-oxidation of Cr(III) under aerobic conditions.

The species of Cr adsorbed on biochar and the changes in surface functional groups of biochar after Cr(VI) removal were investigated using XPS analysis. To avoid interferences from oxygen, sample preparation was performed in an anaerobic glovebox. The samples used for XPS analysis were collected at 24 h from the anaerobic/aerobic kinetics experiments. Approximately 92.2% and 88.9% of the Cr sorbed on MBC was in the form of Cr(III) under anaerobic and aerobic conditions, respectively, greater than that on BC by 89.3% and 76.6% (Fig. 2a, b and Additional file 1: Fig. S7a, b). Given that the quantity of Cr(III) generated in the solution is less than the amount of Cr(VI) removed (Fig. 1a, b), it can be inferred that Cr(VI) is

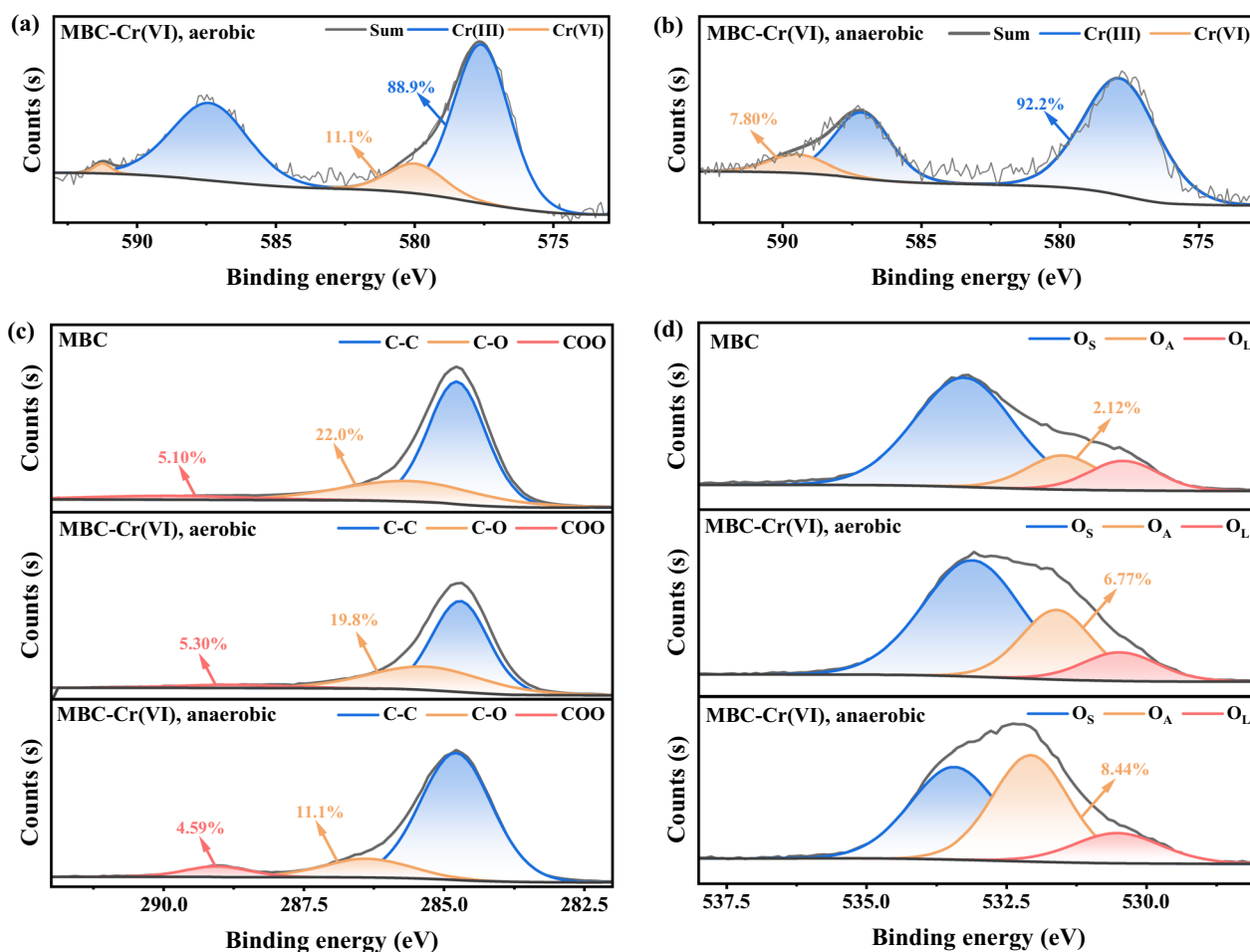


Fig. 2 XPS spectra of MBC. **a, b** Cr 2p XPS spectra under aerobic and anaerobic conditions; **c** C1s XPS spectra; and **d** O1s XPS spectra. O_L, O_A and O_S in panel d represent iron-bound lattice oxygen, surface-adsorbed oxygen, and oxygen banded to the carbon surface, respectively

more susceptible to adsorption followed by reduction, as demonstrated by a prior study (Zhong et al. 2018). In addition, the efficiency of Cr(VI) reduction was investigated by estimating the content of Cr(III) adsorbed on the biochar surface and the Cr(III) generated in the sorbent solution. The proportion of Cr(III) adsorbed by biochar was determined by XPS. The Cr(VI) reduction efficiencies on MBC were 89.8% and 62.2% under anaerobic and aerobic conditions, respectively, greater than those on BC by 32.7% and 49.3%, accounting for 92.5% and 89.4% of Cr(VI) removal (Fig. 1d and Additional file 1: Fig. S4d). The above results indicated that a higher reduction efficiency of Cr(VI) was observed on MBC, especially under anaerobic conditions. Additionally, the micropore volume and pore size distribution of MBC were essentially the same as those of BC (Additional file 1: Fig. S5e, f and Table S3), suggesting that the active species on MBC, rather than the micropores,

mainly facilitated Cr(VI) transformation, as discussed below.

O-containing functional groups on the biochar surface can adsorb or reduce Cr(VI) via complexation or redox processes (Hu et al. 2024; Fei et al. 2022; Zhang et al. 2020). In the O1s spectra, the peaks at 530.4, 531.6 and 533.5 eV are iron-bound lattice oxygen (O_L), surface-adsorbed oxygen (O_A), and oxygen banded to carbon surface (O_S), respectively (Mian et al. 2018; Yang et al. 2016b). The O_A and total O content of MBC after Cr(VI) removal increased from 2.12% to 8.44% and 13.2% to 25.4%, respectively (Fig. 2d and Additional file 1: Table S4), indicating that chromium oxides formed on the MBC surface. In addition, the content of surface reductive C–O groups of MBC decreased by 10.9% after Cr(VI) removal under anaerobic conditions, 4.95 times higher than that of 2.2% under aerobic conditions (Fig. 2c and Additional file 1: Table S4). However, the content of

surface oxidative C=O groups also decreased by 0.51% under anaerobic conditions (Fig. 2c and Additional file 1: Table S4). These results suggested that the reduction of Cr(VI) by surface C–O is limited because phenolics are theoretically oxidized to carboxyl groups, leading to an increase in C=O content (Liu et al. 2020; Zhang et al. 2020). Therefore, these reduced C–O groups were probably released into solution, consistent with the higher C–O intensity of MBC-derived DOM observed in the FTIR spectra (Additional file 1: Fig. S5d).

Magnetite (Fe₃O₄) was successfully loaded onto biochar after α -Fe₂O₃ doping, as shown by energy dispersive spectrometry (EDS), XPS, FTIR, and XRD analyses (Fig. 3 and Additional file 1: Figs. S5 and S8). Before Cr(VI) removal, Fe(II) (710.7 and 724.3 eV), Fe(III) (712.1 and 725.7 eV), and satellite peaks of Fe(II) (715.1 eV) were observed in the Fe 2p_{3/2} XPS spectra of MBC (Fig. 3a). Previous studies have reported that Fe(II) atoms can transfer electrons or diffuse from the internal Fe₃O₄ or Fe₃S₄ to the iron-based surface of the magnetically modified bulk biochar, thus reducing the adsorbed Cr(VI) to Cr(III) (Zhong et al. 2018; Wang et al. 2020). Electron transfer between solid Fe(II) and adsorbed Cr(VI) was obvious under aerobic conditions, with the satellite Fe(II) peaks apparently disappearing and the Fe(III) peaks increasing

from 42.6% to 63.7% after Cr(VI) removal (Fig. 3b). However, the Fe(III) peaks increased slightly from 42.6% to 46.2% after Cr(VI) removal under anaerobic conditions (Fig. 3c), which may be due to a re-reduction of Fe(III) to Fe(II). In addition, MBC released a small amount of ionic Fe(II) (4.33 mg L⁻¹) in the control group [without Cr(VI)], and its surface Fe content decreased from 1.32% to 0.78% after Cr(VI) removal (Additional file 1: Fig. S9 and Table S4). However, no Fe(II) or Fe(III) was detected in the experimental group [with Cr(VI)]. This indicated that the released Fe(II) was immediately oxidized by Cr(VI), and insoluble hydroxide precipitates may have formed via the hydrolysis of Fe(III) or the mixing of Fe(III) oxide with ions, as reported in our recent study (Hu et al. 2024). The stoichiometric ratio between Cr(VI) and Fe(II) without biochar is 1:3 (Xu et al. 2020b). However, the released concentration of Fe(II) in this study (4.33 mg L⁻¹) was much lower than the concentration of Cr(VI) reduced (44.9 mg L⁻¹). Therefore, other reductive substances were involved in the conversion of Cr(VI), because the Fe(II) loaded or released from MBC in this study was not sufficient to reduce such a large amount of Cr(VI).

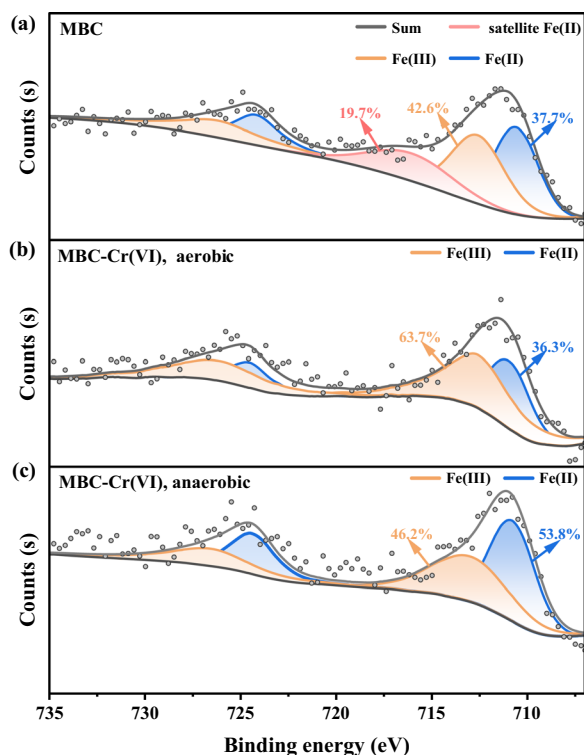


Fig. 3 Fe 2p XPS spectra of MBC. **a** Before Cr(VI) adsorption; **b** after Cr(VI) adsorption under aerobic conditions; **c** after Cr(VI) adsorption under anaerobic conditions

3.2 Influence of bulk PFRs on Cr(VI) transformation

PFRs with delocalized unpaired electrons can engage in direct reactions with contaminants through single-electron transfer. The concentration and type of these radicals predominantly influence the redox reactivity of biochar (Zhu et al. 2020; Ruan et al. 2019). An increase in the concentration of PFRs enhances the electron transfer capability of biochar (Zhu et al. 2020). PFRs are typically classified into three categories: oxygen-centered radicals, carbon-centered radicals, and oxygenated carbon-centered radicals, based on their spectroscopic splitting factors (g values) (Vejerano et al. 2011). Oxygen-centered radicals are represented by semiquinone radicals ($g > 2.0040$), oxygenated carbon-centered radicals by phenoxyl radicals ($g = 2.0030–2.0040$), and carbon-centered radicals by cyclopentadienyls ($g < 2.0030$). Prior studies have demonstrated that a higher g value of PFRs corresponds to a lower electron donation ability (Ruan et al. 2019; Zhong et al. 2018). For instance, carbon-centered radicals (i.e., cyclopentadienyls) possess a potent electron-donating ability to reduce pollutants [such as Cr(VI)] with high redox potential (Zhong et al. 2018), while oxygen-centered radicals (i.e., semiquinone radicals) can function as reversible electron carriers in redox reactions (Xu et al. 2019). In the present study, the bulk PFRs concentration of MBC increased dramatically by 5.6 times compared to that of unmodified BC (Fig. 4a, d and Table 1), indicating that the addition of transition metals significantly promoted bulk PFRs formation (Fang

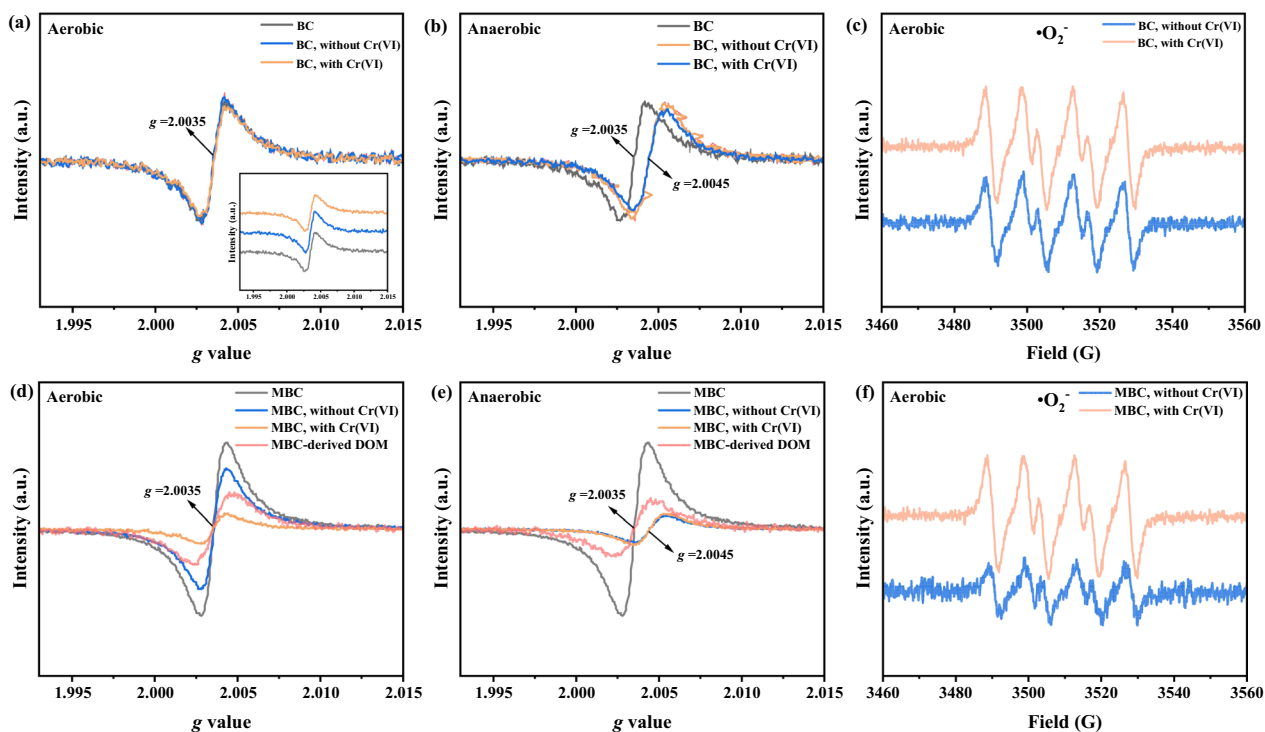


Fig. 4 EPR signals of MBC and BC. Bulk PFRs signals of **a, b** BC and **d, e** MBC under aerobic and anaerobic conditions; $\cdot\text{O}_2^-$ signals of **c** BC and **f** MBC under aerobic conditions after 10 min of sharking in the dark

Table 1 The PFRs properties of BC and MBC

Sample	Condition	10^{18} spins g^{-1}	10^{18} spins $\text{g}^{-1} \text{C}^{-1}$	<i>g</i> value	Radical type
BC	Original ^a	0.639	1.20	2.0035	Phenoxyl
	Aerobic, without Cr(VI)	0.639	–	2.0035	Phenoxyl
	Aerobic, with Cr(VI)	0.595	–	2.0035	Phenoxyl
	Anaerobic, without Cr(VI)	0.471	–	2.0045	Semiquinone
	Anaerobic, with Cr(VI)	0.419	–	2.0045	Semiquinone
MBC	Original ^a	3.56	7.86	2.0035	Phenoxyl
	Aerobic, without Cr(VI)	2.47	–	2.0035	Phenoxyl
	Aerobic, with Cr(VI)	0.608	–	2.0035	Phenoxyl
	Anaerobic, without Cr(VI)	0.448	–	2.0045	Semiquinone
	Anaerobic, with Cr(VI)	0.516	–	2.0045	Semiquinone
MBC-derived DOM	Aerobic, without Cr(VI)	1.33	30.8	2.0035	Phenoxyl
	Anaerobic, without Cr(VI)	1.06	35.7	2.0035	Phenoxyl

^a Original: conditions after pyrolysis

et al. 2015; Vejerano et al. 2011). The *g* values of MBC and BC were 2.0035, suggesting a class of carbon–oxygen-centered PFRs (phenoxyl radicals). This finding implies that $\alpha\text{-Fe}_2\text{O}_3$ doping only altered the concentration of the bulk PFRs on biochar but did not modify the type of PFRs, consistent with results from FeCl_3 -modified biochar in previous studies (Hu et al. 2024; Vejerano et al. 2011). Furthermore, PFRs exhibit properties akin to free

electrons and display a high electron donor capacity, as the *g* value of 2.0035 is close to the *g* factor of free-electron (2.0023) and carbon–oxygen-centered PFRs have low Mulliken charge (0.150 *e*) (Zhong et al. 2018).

The bulk PFRs of MBC and BC showed significantly different EPR signals under anaerobic/aerobic conditions. The concentrations of bulk PFRs for MBC decreased sharply from 3.56×10^{18} spins g^{-1} to 0.448×10^{18} spins g^{-1}

in systems without Cr(VI) and increased slightly to 0.516×10^{18} spins g^{-1} after Cr(VI) treatment under anaerobic conditions (Fig. 4e and Table 1), indicating that these bulk PFRs did not directly participate in Cr(VI) reduction. In addition, the g values of MBC in these systems increased from 2.0035 to 2.0045 both in the presence and absence of Cr(VI), indicating that the PFRs changed from carbon–oxygen-centered (phenoxy radicals) to oxygen-centered (semiquinone radicals) species under anaerobic conditions (Xu et al. 2023). These results suggested that the bulk PFRs on MBC had a lower ability to donate electrons to Cr(VI) under anaerobic conditions. However, the PFRs signals in MBC under aerobic conditions were completely different from those under anaerobic conditions. Under aerobic conditions, the concentration of bulk PFRs for MBC decreased slightly from 3.56×10^{18} spins g^{-1} to 2.47×10^{18} spins g^{-1} in systems without Cr(VI). After Cr(VI) removal, the concentration decreased significantly to 0.608×10^{18} spins g^{-1} (Fig. 4d and Table 1). This suggests that PFRs were consumed by providing electrons to Cr(VI).

In addition to the direct reduction of bulk PFRs, indirect reduction of Cr(VI) can also occur for MBC under aerobic conditions. Superoxide radical ($\cdot O_2^-$) signals were detected in the MBC solutions (Fig. 4f) and disappeared following the addition of BQ (Additional file 1: Fig. S11a). The neutralization of $\cdot O_2^-$ with BQ (100 mM) led to a decrease in Cr(VI) removal efficiency from 69.6% to 60.9% within 24 h (Additional file 1: Fig. S11d), suggesting an indirect reduction of Cr(VI) by PFRs transferring electrons to O_2 to generate $\cdot O_2^-$, consistent with a previous study (Xu et al. 2020a). Moreover, hydroxyl radical ($\cdot OH$) and singlet oxygen (1O_2) signals were also detected in the MBC solutions under aerobic conditions and disappeared following the addition of IPA and FFA, respectively (Additional file 1: Figs. S10 and S11). These $\cdot OH$ (2.8 eV) and 1O_2 (1.88 eV) are capable of re-oxidizing the generated Cr(III) to Cr(VI). However, quenching $\cdot OH$ with IPA (100 mM) decreased the Cr(VI) removal efficiency from 69.6% to 65.8% (Additional file 1: Fig. S11d), potentially due to the fact that IPA can also neutralize the PFRs, thus resulting in a lower removal of Cr(VI). A prior study reported that PFRs on biochar were easily extracted by polar solvents such as methanol, dichloromethane, and IPA (Fang et al. 2014). Terephthalic acid (TPA, 50 μM) was further used to neutralize $\cdot OH$ (Liu et al. 2022), and marginally increased the removal of Cr(VI) to 70.9% (Additional file 1: Fig. S11d). Similarly, FFA (100 mM) was used to neutralize 1O_2 (Liu et al. 2022), and the Cr(VI) removal efficiency increased to 74.6% (Additional file 1: Fig. S11d). These quenching results indicated that $\cdot OH$ and 1O_2 can re-oxidize Cr(III) under aerobic conditions, resulting in low Cr(VI)

removal efficiency. This could explain the phenomenon that the decrease in Cr(III) concentrations was higher under aerobic conditions than under anaerobic conditions. Similar results were observed for BC (Fig. 4a–c). The above results indicated that the bulk PFRs on MBC and BC were directly or indirectly involved in Cr(VI) reduction under aerobic conditions, while the generation of $\cdot OH$ and 1O_2 could also hinder the reduction of Cr(VI). However, the bulk PFRs on MBC and BC had little effect on Cr(VI) reduction under anaerobic conditions.

Organic functional groups containing unpaired electrons (such as PFRs) in biochar could be present in the form of DOM that participated in Cr(VI) reduction (Dong et al. 2014). Evidently, phenoxy PFRs was detected in DOM derived from MBC under anaerobic conditions (Fig. 4e). Although the concentration of PFRs in the DOM (1.06×10^{18} spins g^{-1}) was lower than bulk biochar (3.56×10^{18} spins g^{-1}), its carbon content (2.97%) was also significantly less than bulk biochar (45.3%) (Table 1 and Additional file 1: Table S3). Given that PFRs are organic radicals, we correlated the PFRs concentration to its carbon content. The PFRs/C in DOM was 35.7×10^{18} spins $g^{-1} C^{-1}$ (Table 1), much higher than in bulk MBC (7.86×10^{18} spins $g^{-1} C^{-1}$), indicating a superior electron transfer capacity of DOM. Previous research also suggested that the active intermediates in the DOM electron transfer process primarily consist of electron-rich phenoxy radicals (Remke et al. 2022, 2023). Additionally, compared to bulk PFRs, these dissolved PFRs increased contact sites with contaminants and thus resulted in higher reactivity (Lian et al. 2020). Moreover, humic acids with high aromatic carbon content are more susceptible than fulvic acids to forming these dissolved PFRs (Jacobs et al. 2012). Biochar produced at 500 °C contains a high aromatic carbon content of over 90%, according to our prior studies (Hu et al. 2019, 2021). Therefore, these abundant dissolved PFRs derived from MBC may play an important role in the reduction of Cr(VI). We further analyzed these dissolved PFRs by EEM and FTICR-MS.

3.3 UV–vis and fluorescence evidence of dissolved PFRs involved in Cr(VI) transformation

PFRs in DOM released by biochar can directly transfer electrons to reduce Cr(VI) to Cr(III), resulting in changes in the photochemical properties of the solution (Dong et al. 2014; Chen et al. 2021). Since the dissolved PFRs could not be isolated from the DOM, we characterized the DOM instead of the dissolved PFRs. UV–vis spectroscopy can be used to reflect the chemical composition of DOM, and the Napierian absorption coefficient (m^{-1}) was calculated (detailed in Additional file 1: Text

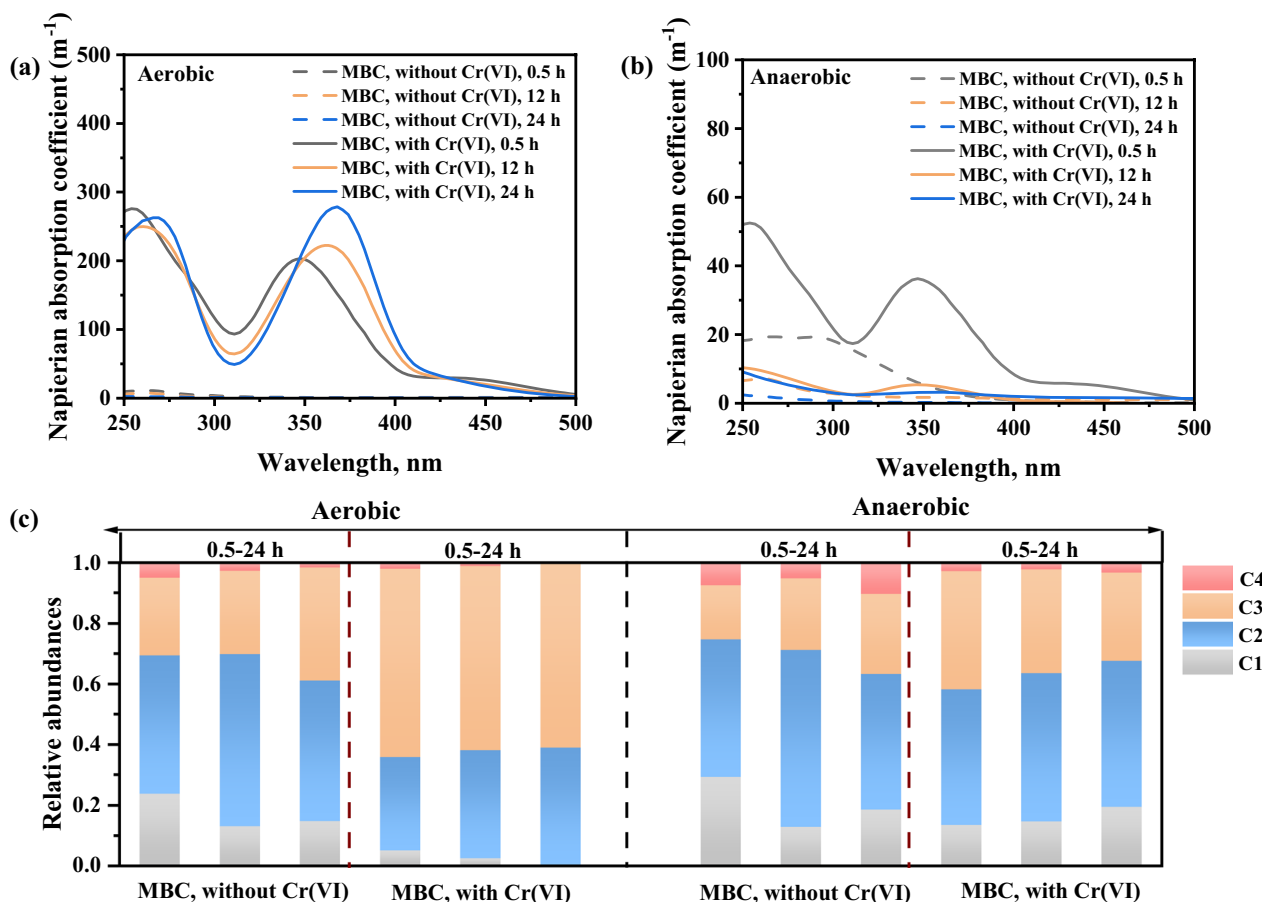


Fig. 5 UV-vis spectra of MBC under **a** aerobic and **b** anaerobic conditions. **c** The relative contributions of the PARAFAC components of MBC

S4). The UV-vis absorbance intensities of the MBC solution in systems with Cr(VI) increased under both anaerobic and aerobic conditions and were much higher than those of systems without Cr(VI) (Fig. 5a, b). Two spectral regions, 250–300 nm and 320–450 nm, showed significant changes in systems with Cr(VI). Similar results were observed for the absorbance of BC-derived DOM (Additional file 1: Fig. S12). It is noted that these two regions were more involved in DOM-Cr(VI) binding interactions (Mu et al. 2022). Generally, the 230–300 nm spectral region is associated with conjugated carboxylic groups, while the 300–450 nm spectral region reflects the absorption characteristics of both phenolic and carboxylic groups (Habibul and Chen 2018).

Compared to the significant increase in DOM absorbance at 250–450 nm for MBC under aerobic conditions, the value at 250–450 nm was slightly increased under anaerobic conditions. The low concentration of electron acceptors (Cr(VI), 1.45 mg L⁻¹) in the MBC system under anaerobic conditions can explain the small change in absorbance, as Mu et al. (2022) reported that

the absorbance of a solution was highly related to Cr(VI) concentration. In addition, with increasing reaction time, the wavelengths of the highest peaks in the 250–300 nm and 320–450 nm regions of MBC increased from 254 to 272 nm and 347 nm to 371 nm, respectively. These observations suggested that DOM interacted with Cr(VI) to generate compounds with higher degrees of unsaturation or greater amounts of conjugation, which contributed to the absorbance redshift (Mu et al. 2022; Worms et al. 2019). In addition, the formation of DOM-Fe complexes was probably responsible for a slight increase in the absorbance of MBC under anaerobic conditions in the Cr(VI)-free systems (Fig. 5b and Additional file 1: Fig. S13) (Jia et al. 2021; Kim et al. 2019). Bianco et al. (2014) revealed that electron transfer of L-tryptophan, L-tyrosine, and 4-phenoxyphenol occurred after irradiation ≥ 8 h, resulting in an increase in the spectrum above 330–350 nm. Phillips and Smith (2015) reported that the adsorption spectrum of fulvic acid decreased at 250–400 nm after reduction by NaBH₄. Therefore, the absorbance spectrum of DOM changes when electron transfer occurs.

Visual and quantitative estimation of DOM components was performed by EEM fluorescence spectroscopy and PARAFAC analysis (Jia et al. 2021; Zhang et al. 2019). The fluorescence spectra of MBC solutions showed significant quenching after Cr(VI) removal (Additional file 1: Figs. S14 and S15), indicating that DOM has a strong capacity to bind Cr(VI) (Mu et al. 2022; Zhang et al. 2021). Four components (referred to as C1, C2, C3, and C4) were identified by PARAFAC analysis (Additional file 1: Fig. S16). The C1, C2, and C3 components (Em/Ex=284/263 nm, 315/275 nm, 306/263 nm, respectively) were classified as protein-like substances (Coble 2007). The C4 component (Em/Ex=411/<250, 302 nm) was characterized as a low molecular weight UVA humic-like component (Stedmon and Markager 2005). In systems without Cr(VI), the relative intensity of the protein-like components (C1–C3) was higher in MBC than in BC (Additional file 1: Fig. S17), suggesting that the addition of α -Fe₂O₃ changed the composition of DOM (Jia et al. 2021). In systems with Cr(VI), the relative intensities of C1 and C4 for MBC decreased significantly, and those of C1, C2, and C4 for BC dropped markedly after the removal of Cr(VI) (Fig. 5c and Additional file 1: Fig. S17). This suggested that these components tend to bind Cr(VI) and may participate in Cr(VI) reduction. The protein-like components contain reducing groups, such as amino groups and phenolic groups, which allow the reduction of Cr(VI) to Cr(III) (Mu et al. 2022). The absorption and fluorescence spectra of DOM indicated that protein-like and humic-like components of DOM were involved in Cr(VI) reduction, and these components may be the main species of PFRs, including conjugated carboxylic groups and phenolic groups. Subsequent FTICR-MS analysis verified the specific components of these dissolved PFRs.

3.4 Molecular evidence of dissolved PFRs involved in Cr(VI) transformation

The molecular composition of MBC-derived DOM changed significantly under anaerobic conditions, with the average DOM formula changing from C_{21.1}H_{26.0}O_{5.25}N_{0.31}S_{0.47} to C_{22.3}H_{28.3}O_{6.79}N_{0.91}S_{0.45} after Cr(VI) removal (Additional file 1: Table S5). In addition, a significant increase in molecular weight (MW_w) and double-bond equivalents (DBE_w) indicated the formation of molecules of larger sizes and more unsaturated compounds, consistent with the increased absorbance shown in Fig. 5a, b. Three categories were established: the formulas removed from DOM after Cr(VI) removal (F1), the formulas remaining before and after Cr(VI) removal (F2), and newly produced formulas after Cr(VI) removal (F3). The C_w, MW_w, DBE_w, and modified aromaticity index (AI_{mod,w}) values of MBC increased from 22.9 to 29.2, 423 to 541, 9.40 to 13.5, and 0.27 to 0.37 (F1 vs. F3), respectively (Additional file 1: Table S5), indicating that DOM compounds with higher MW and degrees of unsaturation were formed; additionally, a higher aromatic index was obtained. Moreover, the proportions of CHO and CHOS compounds for MBC-derived DOM decreased after Cr(VI) removal, while the proportions of CHON and CHONS compounds increased (Additional file 1: Table S5). These results suggested that CHO and CHOS compounds were mainly involved in Cr(VI) transformation, while CHON and CHONS compounds were likely retained in DOM after Cr(VI) removal.

Reductive soluble sulfur compounds can effectively reduce Cr(VI) to Cr(III) in soil remediation (Yang et al. 2021). Higher proportions of CHOS compounds and dissolvable sulfate content were observed in MBC-derived DOM than in BC-derived DOM, especially under anaerobic conditions (Additional file 1: Fig. S18a and Table S5). These results showed that α -Fe₂O₃

Table 2 Molecular parameters for CHO and CHOS compounds of MBC-derived DOM

Compound	Category	Percentage	C _w	H _w	O _w	S _w	MW _w	DBE _w	AI _{mod,w}	NOSC _w
Aerobic										
CHO	F1 ^a	26.9	22.9	22.4	4.73	0.00	372	12.7	0.43	-0.48
	F3 ^b	16.2	26.6	29.9	8.87	0.00	490	12.6	0.37	-0.39
CHOS	F1	31.6	23.3	29.4	6.77	1.45	463	9.65	0.28	-0.46
	F3	24.8	25.6	31.1	6.81	1.25	486	11.1	0.30	-0.51
Anaerobic										
CHO	F1	31.9	23.0	26.3	4.11	0.00	367	10.9	0.36	-0.82
	F3	10.9	29.4	38.2	5.52	0.00	479	11.3	0.34	-0.80
CHOS	F1	35.8	23.2	29.5	6.14	1.23	445	9.49	0.25	-0.43
	F3	22.6	29.8	31.1	7.79	1.41	557	15.2	0.40	-0.33

^a F1: the removed formulas in DOM after Cr(VI) removal

^b F3: the newly produced formulas in DOM after Cr(VI) removal

doping increased the release of S-containing compounds. In addition, the proportions of F1 and F3 for CHOS compounds for MBC were higher than those of CHO compounds (Table 2), suggesting that CHOS compounds were mainly involved in Cr(VI) reduction. Among these S-containing compounds, 31.6% of the CHOS formulas in F1 for MBC showed O/S ratios < 4 (Fig. 6a). In addition, $C_{17}H_{28}O_3S$ and $C_{18}H_{30}O_3S$ were the dominant molecules in the CHOS compounds of MBC before Cr(VI) removal (Additional file 1: Fig. S18b). The above findings indicated that MBC contained a high proportion of highly reduced-S compounds (Song et al. 2018). After Cr(VI) removal, these

highly reduced-S compounds decreased to 27.6% in F3 for MBC, suggesting the oxidation of low O/S CHOS compounds to highly oxygenated sulfides, especially those with O/S ratios above 6 (Fig. 6a). The nominal carbon oxidation state (NOSC) describes the average C oxidation state per formula and is expected to respond to DOM redox changes (Wang et al. 2019; Patel et al. 2021). The NOSC_w value of F3 categories for CHOS compounds of MBC under anaerobic conditions was -0.33, and was higher than -0.43 of F1 categories, further indicating that the newly formed compounds in DOM were more oxidized as a result of electron donating to Cr(VI) (Table 2).

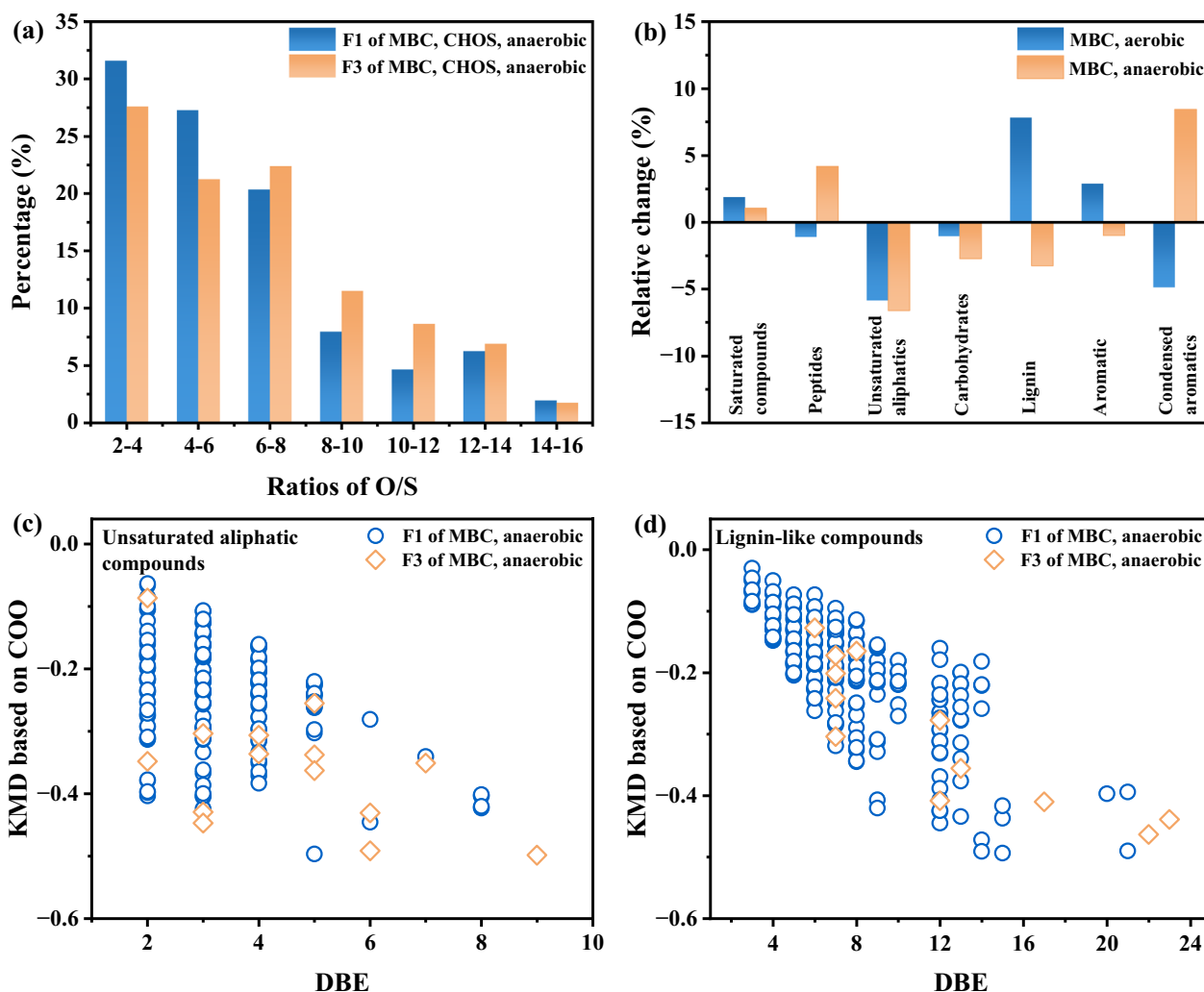


Fig. 6 **a** Classification of CHOS species in the removed formulas (F1) and newly produced formulas (F3) categories of MBC-derived DOM according to the ratios of O/S in their molecules. **b** Relative changes in compound classes between the MBC-derived DOM before and after reaction with Cr(VI). The relative change was calculated by subtracting the percentage of a compound class in the MBC-derived DOM from the percentage of the compound class in the DOM after reactions with Cr(VI). COO-based Kendrick mass defect (KMD) vs. DBE for the **c** unsaturated aliphatic compounds and **d** lignin-like compounds in CHO compounds of MBC-derived DOM

The changes in the composition of the major compound classes were further analyzed by calculating the relative changes in the percentages of the compound classes after the reactions (Fig. 6b and Additional file 1: Fig. S19). Under anaerobic conditions, a significant decrease in the unsaturated aliphatic compounds and lignin-like compounds was observed after Cr(VI) removal by MBC-derived DOM, indicating that these compounds could react with Cr(VI) (Fig. 6b). Unsaturated aliphatic compounds contain a number of unsaturated acids, such as monocarboxylic acids and binary carboxylic acids, which can promote the conversion of Cr(VI) by electron transfer (Xu et al. 2019; Fei et al. 2022). Similarly, lignin-like compounds were oxidized by Cr(VI). Unsaturated and hydroxylated aliphatic carboxylic acids are involved in the first step in lignin oxidation, and the generated conjugated unsaturated (hydroxylated) acids can undergo aromatization and condensation to form condensed aromatic structures (Waggoner et al. 2015; Waggoner and Hatcher 2017). As expected, a significant increase in condensed aromatic compounds was observed in MBC-derived DOM after Cr(VI) removal (Fig. 6b).

A series of Kendrick Mass Defect (KMD) analyses were performed to identify the major active species reducing Cr(VI). According to the KMD definition, formulas with the same KMD value differ only in multiples of the selected mass corresponding to atoms or functional groups, such as O, H₂, or COOH (Zeng et al. 2020). As shown in Fig. 6c, d, the regular -COO spacing pattern in unsaturated aliphatic compounds and lignin-like compounds reflected the presence of abundant polycarboxylic, conjugated carboxylic, and/or carboxylic acid ester groups in DOM prior to Cr(VI) removal. However, the amounts of -COO compounds with low DBE values decreased significantly, while some -COO compounds with high DBE values were produced after Cr(VI) removal. These results indicated that most of the

molecules were carboxyl-substituted and that decarboxylation may be an important reaction between DOM and Cr(VI). A loss of carboxyl groups can lead to the formation of organic radicals that can sacrifice hydrogen and undergo aromatization and condensation to form condensed aromatic structures (Waggoner et al. 2015; Waggoner and Hatcher 2017), consistent with the increased absorbance at 250–450 nm (Fig. 5). Moreover, single electron transfer reactions of organic molecules with strong reductivity are more favorable under anaerobic conditions due to the lower Eh values of the solution (Additional file 1: Fig. S6).

In contrast, under aerobic conditions, after reaction with Cr(VI), MBC-derived DOM decreased the content of unsaturated aliphatic compounds and condensed aromatic compounds and increased the content of saturated compounds, lignin-like compounds, and aromatic/polyphenol compounds (Fig. 6b). Phenols are expected to promote Cr(VI) reduction because of their strong correlation with electron donor capacity (Lv et al. 2018). In this study, a portion of the condensed hydrocarbons was ionized, and these compounds with high DBE values were more prone to attack by ·OH or ¹O₂ in solution (Additional file 1: Fig. S10), leading to the formation of lignin-like or aromatic compounds by ring-opening. Westerhoff et al. (1999) first reported that ·OH tends to attack the aromatic carbon structure in DOM. Our recent study also showed that ·OH prefers to react with unsaturated bonds through addition reactions during oxidation (Zhuo et al. 2019). Additionally, aliphatic and saturated compounds can promote ¹O₂ formation (Zeng et al. 2020), consistent with the higher EPR signals of ¹O₂ in solution after Cr(VI) removal (Additional file 1: Fig. S10). Moreover, in DOM-only systems where the dissolved organic carbon content was approximately 8.0 mg L⁻¹, the Cr(VI) removal efficiency by MBC-derived DOM under anaerobic conditions was 3.93 times

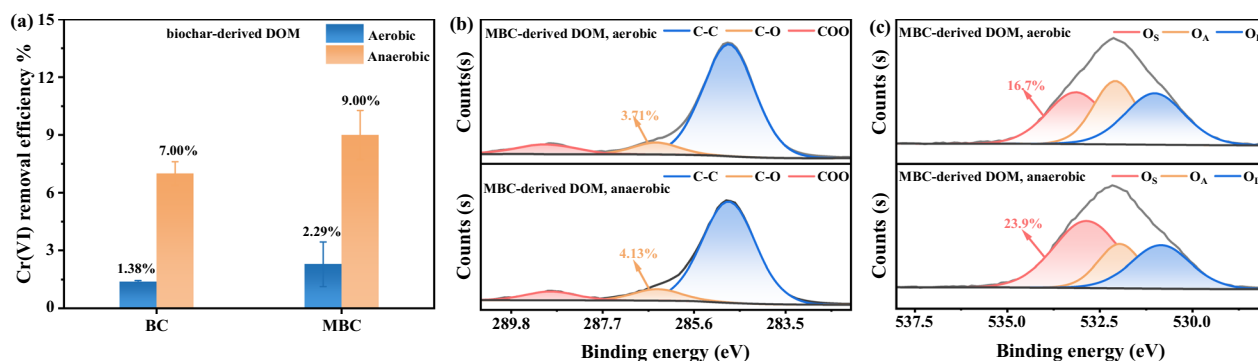
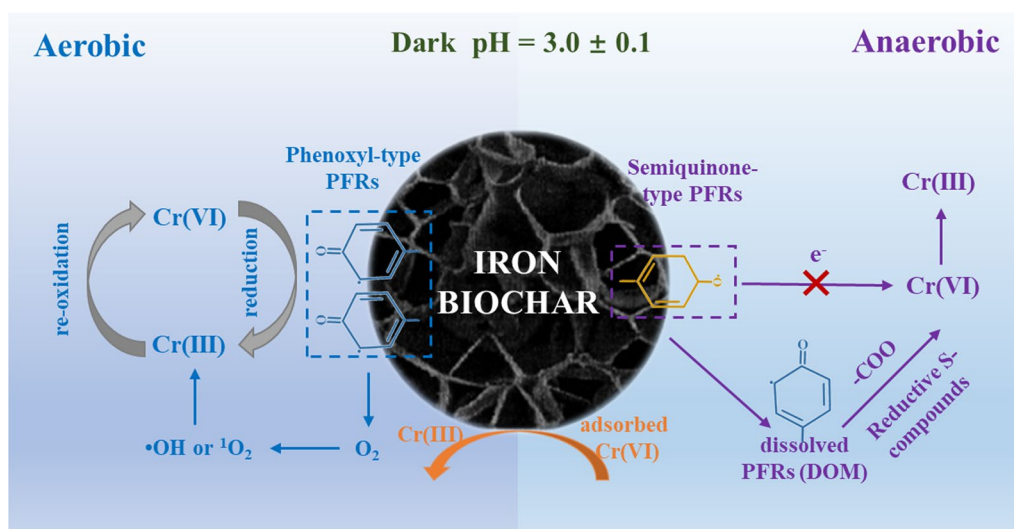


Fig. 7 a Cr(VI) removal efficiencies for biochar-derived DOM. The initial Cr(VI) concentration was 50 mg L⁻¹. The initial pH was 3.0 ± 0.1. b C1s and c O1s XPS spectra of MBC-derived DOM



Scheme 1 Schematic illustration of Cr(VI) reduction pathways by MBC

higher than that under aerobic conditions (Fig. 7a). Furthermore, DOM derived from MBC under anaerobic conditions contained higher S/C ratio and oxygen-rich functional groups (Additional file 1: Table S3 and Fig. 7b, c). These results further demonstrated the high electron transfer capability of dissolved PFRs for Cr(VI) reduction under anaerobic conditions.

3.5 Mechanistic insights

The mechanisms of Cr(VI) transformation by MBC-derived PFRs are shown in Scheme 1. The bulk PFRs on MBC showed little effect on Cr(VI) reduction under anaerobic conditions, as the PFRs changed from a high concentration of phenoxyl radicals with high reducing activity to a low concentration of semiquinone radicals with low reducing activity. The dissolved PFRs containing high contents of phenoxyl radicals released by MBC promoted Cr(VI) reduction. Additional FT-ICR MS analysis showed that low O/S ($O/S < 4$) reductive S-containing compounds and $-COO$ in the unsaturated aliphatic and lignin-like compounds of the dissolved PFRs dominated the reduction of Cr(VI). In contrast, the bulk PFRs on MBC promoted the reduction of Cr(VI) by direct electron transfer or indirect formation of $\cdot O_2^-$ under aerobic conditions. However, the reduced Cr(III) could be re-oxidized due to the presence of large amounts of ROS ($\cdot OH$ and 1O_2) in solution.

4 Conclusion

This study highlights the importance of $\alpha-Fe_2O_3$ -modified biochar in remediating Cr(VI) in anaerobic environments and the potential impact of dissolved PFRs

on Cr(VI) reduction. Compared to unmodified biochar, $\alpha-Fe_2O_3$ incorporation increased the concentration of phenoxyl radicals by 5.6 times, thereby enhancing Cr(VI) transformation. In addition, $\alpha-Fe_2O_3$ -doped biochar was more efficient in reducing Cr(VI) under anaerobic conditions than under aerobic conditions due to the release of dissolved PFRs, which have high reactivity and accessibility. Additional FTICR-MS analysis indicated that reduced S compounds ($O/S < 4$) and carboxylic acid ($-COO$) groups in the unsaturated aliphatic and lignin-like compounds in dissolved PFRs were the potential major active species accelerating Cr(VI) reduction under anaerobic conditions. In contrast, under aerobic conditions, these dissolved PFRs promoted the generation of $\cdot OH$ and 1O_2 , which in turn re-oxidized the reduced Cr(III). Based on our work, we recommend that the reactivity of dissolved PFRs in iron-biochar be considered in anaerobic environments such as paddy soils. This study provides new insights into the role of dissolved PFRs from iron-modified biochar in promoting Cr(VI) reduction in flooded paddy soils.

Supplementary Information

The online version contains supplementary material available at <https://doi.org/10.1007/s42773-024-00305-6>.

Additional file 1: Text S1. Characterization of biochar and iron-biochar. **Text S2.** Concentration analysis. **Text S3.** Sorption models. **Text S4.** UV-vis and fluorescence properties. **Text S5.** Data processing. **Text S6.** Results and discussion of Cr(VI) removal kinetics and sorption isotherms models. **Figure S1.** The residual analysis of the excitation and emission wavelength of 2- to 7-components PARAFAC model for the dissolved organic carbon of BC and MBC. **Figure S2.** Sum of squared error (SSE) and core consistency of each PARAFAC of the dissolved organic carbon model ($n = 40$). **Figure S3.** Split analysis of 4-component PARAFAC model

with the split style $S_4C_6T_3$ for all EEMs of DOM from the BC and MBC.

Figure S4. **a** Cr(VI) removal kinetics, **b** Cr(III) generation kinetics, **c** Cr(VI) adsorption isotherms, and **d** Cr(VI) removal and reduction efficiencies for BC. **Figure S5.** **a** Zeta potential, **b** XRD, **c** FTIR, **e** CO₂ adsorption, and **f** nanopore size distribution of BC and MBC. **Figure S6.** **a, b** pH and **c, d** Eh values of BC and MBC under aerobic and anaerobic conditions. **Figure S7.** XPS spectra of BC. **a, b** Cr 2p XPS spectra under aerobic and anaerobic conditions; **c** C1s XPS spectra; and **d** O1s XPS spectra. O_A and O_S in panel d represent surface-adsorbed oxygen and oxygen banded to the carbon surface, respectively. **Figure S8.** Morphological characterization of biochar. **a–c** SEM images of BC; **d–f** SEM images of MBC; **g** energy dispersive spectroscopy mapping images of MBC. **Figure S9.** The concentration of Fe(II) released by MBC in the absence of Cr(VI) under aerobic and anaerobic conditions. **Figure S10.** EPR signals of ¹O₂ and [•]OH in the solution of BC and MBC. **Figure S11.** EPR signals of **a** [•]O₂[−], **b** ¹O₂ and **c** [•]OH in the solution of MBC under aerobic conditions with the addition of scavengers of BQ, IPA, and FFA, respectively. **d** The Cr(VI) removal efficiency with different added scavengers. The initial Cr(VI) concentration was 50 mg L^{−1}. The initial pH was 3.0 ± 0.1. **Figure S12.** UV–vis spectra of BC solutions under **a** aerobic and **b** anaerobic conditions. **Figure S13.** DOC concentrations in control and Cr(VI) system of **a** BC and **b** MBC solutions. **Figure S14.** Fluorescence spectra of BC and MBC solutions before and after Cr(VI) removal at 24 h under aerobic conditions. **Figure S15.** Fluorescence spectra of BC and MBC solutions before and after Cr(VI) removal at 24 h under anaerobic conditions. **Figure S16.** EEM of the four fluorescence components identified by PARAFAC analysis. **Figure S17.** The relative contributions of each PARAFAC component to BC and MBC. **Figure S18.** **a** Concentration of dissolvable SO₄^{2−} for BC and MBC. **b** Molecular intensity of CHOS compounds for MBC under anaerobic conditions before Cr(VI) removal. **Figure S19.** Relative changes in compound classes between the BC-derived DOM before and after reaction with Cr(VI). The relative change was calculated by subtracting the percentage of a compound class in the BC-derived DOM from the percentage of the compound class in the DOM after reactions with Cr(VI). **Table S1.** Kinetic parameters of pseudo-first-order and pseudo-second-order models for Cr(VI) removal by BC and MBC under aerobic and anaerobic conditions. **Table S2.** Parameters of Langmuir and Freundlich models for Cr(VI) adsorption by BC and MBC under aerobic and anaerobic conditions. **Table S3.** Elemental, nanopore and pH properties of BC and MBC. **Table S4.** Surface elemental properties of biochar samples before and after Cr(VI) removal determined by XPS. **Table S5.** Molecular parameters of BC and MBC before and after Cr(VI) removal under aerobic and anaerobic conditions.

Acknowledgements

This work was supported by the National Natural Science Foundation of China (42025705 and 42107046), the GDAS' Project of Science and Technology Development (2022GDASZH-2022010105 and 2020GDASYL-202001102019), and the Guangdong Basic and Applied Basic Research Foundation (2021A1515011540). The authors would like to thank "SPRINGER NATURE Author Services" for the language editing.

Author contributions

SH: investigation, methodology, data curation, funding acquisition, writing—original draft. CL: conceptualization, project administration, funding acquisition, writing—review and editing. HB: writing—review and editing, funding acquisition. MC: writing—review and editing. JT: writing—review and editing, formal analysis, software. BJ: software. YR: writing—review and editing. All authors read and approved the final manuscript.

Funding

This work was supported by the National Natural Science Foundation of China (42025705 and 42107046), the GDAS' Project of Science and Technology Development (2022GDASZH-2022010105 and 2020GDASYL-202001102019), and the Guangdong Basic and Applied Basic Research Foundation (2021A1515011540).

Availability of data and materials

The datasets generated during and/or analyzed during the current study are available from the corresponding author on reasonable request.

Declarations

Competing interests

There are no competing interests to declare.

Author details

¹National-Regional Joint Engineering Research Center for Soil Pollution Control and Remediation in South China, Guangdong Key Laboratory of Integrated Agro-environmental Pollution Control and Management, Institute of Eco-environmental and Soil Sciences, Guangdong Academy of Sciences, Guangzhou 510650, China. ²State Key Laboratory of Environmental Geochemistry, Institute of Geochemistry, Chinese Academy of Science, Guiyang 550081, China. ³Chongqing Institute of Green and Intelligent Technology, Chinese Academy of Sciences, Chongqing 400714, China. ⁴School of Environmental Science and Engineering, Guangdong University of Technology, Guangzhou 510006, China. ⁵Guangzhou Institute of Geochemistry, Chinese Academy of Sciences, Guangzhou 510640, China.

Received: 26 September 2023 Revised: 27 January 2024 Accepted: 3 February 2024

Published online: 20 February 2024

References

- Bianco A, Minella M, De Laurentiis E, Maurino V, Minero C, Vione D (2014) Photochemical generation of photoactive compounds with fulvic-like and humic-like fluorescence in aqueous solution. *Chemosphere* 111:529–536. <https://doi.org/10.1016/j.chemosphere.2014.04.035>
- Chen N, Cao SY, Zhang L, Peng X, Wang XB, Ai ZH, Zhang LZ (2021) Structural dependent Cr(VI) adsorption and reduction of biochar: hydrochar versus pyrochar. *Sci Total Environ* 783:147084. <https://doi.org/10.1016/j.scitotenv.2021.147084>
- Coble PG (2007) Marine optical biogeochemistry: the chemistry of ocean color. *Chem Rev* 107:402–418. <https://doi.org/10.1021/cr050350+>
- Cuong DV, Wu PC, Chen L, Hou CH (2021) Active MnO₂/biochar composite for efficient As(III) removal: insight into the mechanisms of redox transformation and adsorption. *Water Res* 188:116495. <https://doi.org/10.1016/j.watres.2020.116495>
- Dittmar T, Koch B, Hertkorn N, Kattner G (2008) A simple and efficient method for the solid-phase extraction of dissolved organic matter (SPE-DOM) from seawater. *Limnol Oceanogr Methods* 6:230–235. <https://doi.org/10.4319/lom.2008.6.230>
- Dong XL, Ma LQ, Gress J, Harris W, Li YC (2014) Enhanced Cr(VI) reduction and As(III) oxidation in ice phase: important role of dissolved organic matter from biochar. *J Hazard Mater* 267:62–70. <https://doi.org/10.1016/j.jhazmat.2013.12.027>
- Fang GD, Gao J, Liu C, Dionysion DD, Wang Y, Zhou DM (2014) Key role of persistent free radicals in hydrogen peroxide activation by biochar: implications to organic contaminant degradation. *Environ Sci Technol* 48(3):1902–1910. <https://doi.org/10.1021/es4048126>
- Fang GD, Liu C, Gao J, Dionysion DD, Zhou DM (2015) Manipulation of persistent free radicals in biochar to activate persulfate for contaminant degradation. *Environ Sci Technol* 49:5645–5653. <https://doi.org/10.1021/es5061512>
- Fei YH, Li MZ, Ye ZF, Guan JY, Huang ZH, Xiao TF, Zhang P (2022) The pH-sensitive sorption governed reduction of Cr(VI) by sludge derived biochar and the accelerating effect of organic acids. *J Hazard Mater* 423:127205. <https://doi.org/10.1016/j.jhazmat.2021.127205>
- Guan FY, Wen JL, Liu JY, Zhou SG, Yuan Y (2023) Simple colorimetric assay for quantification of persistent free radicals in biochars. *Environ Sci Technol Lett* 10:46–51. <https://doi.org/10.1021/acs.estlett.2c00816>
- Habibul N, Chen W (2018) Structural response of humic acid upon binding with lead: a spectroscopic insight. *Sci Total Environ* 643:479–485. <https://doi.org/10.1016/j.scitotenv.2018.06.229>
- Han HW, Song PZ, Cai ZS, Dong WJ, Khan A, Yang K, Fang YT, Liu P, Masek O, Li XK (2022) Immobilizing chromate reductase NfoR on magnetic biochar reduced Cr(VI) in copper-containing wastewater. *J Clean Prod* 361:132118. <https://doi.org/10.1016/j.jclepro.2022.132118>

- Hu SJ, Zhang DN, Yang Y, Ran Y, Mao JD, Chu WY, Cao XY (2019) Effects of the chemical structure, surface, and micropore properties of activated and oxidized black carbon on the sorption and desorption of phenanthrene. *Environ Sci Technol* 53(13):7683–7693. <https://doi.org/10.1021/acs.est.9b01788>
- Hu SJ, Xu DC, Kong XL, Gong J, Yang Y, Ran Y, Mao JD (2021) Effect of the structure and micropore of activated and oxidized black carbon on the sorption and desorption of nonylphenol. *Sci Total Environ* 761:144191. <https://doi.org/10.1016/j.scitotenv.2020.144191>
- Hu SJ, Liu CS, Bu HL, Chen MJ, Fei YH (2024) Efficient reduction and adsorption of Cr(VI) using FeCl₃-modified biochar: synergistic roles of persistent free radicals and Fe(II). *J Environ Sci* 137:626–638. <https://doi.org/10.1016/j.jes.2023.03.011>
- Jacobs LE, Weavers LK, Houtz EF, Chin YP (2012) Photosensitized degradation of caffeine: role of fulvic acids and nitrate. *Chemosphere* 86:124–129. <https://doi.org/10.1016/j.chemosphere.2011.09.052>
- Jia LX, Wu WZ, Zhang J, Wu HM (2021) Insight into heavy metals (Cr and Pb) complexation by dissolved organic matters from biochar: impact of zero-valent iron. *Sci Total Environ* 793:148469. <https://doi.org/10.1016/j.scitotenv.2021.148469>
- Kim HB, Kim JG, Kim SH, Kwon EE, Baek K (2019) Consecutive reduction of Cr(VI) by Fe(II) formed through photo-reaction of iron-dissolved organic matter originated from biochar. *Environ Pollut* 253:231–238. <https://doi.org/10.1016/j.envpol.2019.07.026>
- Klöpffel L, Keiluweit M, Kleber M, Sander M (2014) Redox properties of plant biomass-derived black carbon (biochar). *Environ Sci Technol* 48:5601–5611. <https://doi.org/10.1021/es500906d>
- Lian F, Yu WC, Zhou QX, Gu SG, Wang ZY, Xing BS (2020) Size matters: nano-biochar triggers decomposition and transformation inhibition of antibiotic resistance genes in aqueous environments. *Environ Sci Technol* 54:8821–8829. <https://doi.org/10.1021/acs.est.0c02227>
- Liang S, Zhu LY, Hua J, Duan WJ, Yang PT, Wang SL, Wei CH, Liu CS, Feng CH (2020) Fe²⁺/HClO reaction products produces FeIVO²⁺: an enhanced advanced oxidation process. *Environ Sci Technol* 54:6406–6414. <https://doi.org/10.1021/acs.est.0c00218>
- Liang L, Chen GY, Zhao JH, Shao PH, Li N, He MT, Fu QL, Yan BB, Hou LA (2023) Overlooked composition of natural organic matter conversion in a Fe(II)-induced peroxymonosulfate activation system for river water remediation. *Sci Total Environ* 872:162217. <https://doi.org/10.1016/j.scitotenv.2023.162217>
- Liu JW, Jiang JG, Meng Y, Aihemaiti A, Xu YW, Xiang HL, Gao YC, Chen XJ (2020) Preparation, environmental application and prospect of biochar-supported metal nanoparticles: a review. *J Hazard Mater* 388:122026. <https://doi.org/10.1016/j.jhazmat.2020.122026>
- Liu K, Li FB, Tian QW, Nie CR, Ma YB, Zhu ZL, Fang LP, Huang YY, Liu SW (2021) A highly porous animal bone-derived char with a superiority of promoting nZVI for Cr(VI) sequestration in agricultural soils. *J Environ Sci* 104:27–39. <https://doi.org/10.1016/j.jes.2020.11.031>
- Liu YF, Wang ML, Yin SJ, Xie LK, Qu XL, Fu HY, Shi Q, Zhou F, Xu FL, Tao S, Zhu DQ (2022) Comparing photoactivities of dissolved organic matter released from rice straw-pyrolyzed biochar and composted rice straw. *Environ Sci Technol* 56:2803–2815. <https://doi.org/10.1021/acs.est.1c08061>
- Lv JT, Zhang SZ, Wang SS, Luo L, Cao D, Christie P (2016) Molecular-scale investigation with ESI-FT-ICR-MS on fractionation of dissolved organic matter induced by adsorption on iron oxyhydroxides. *Environ Sci Technol* 50:2328–2336. <https://doi.org/10.1021/acs.est.5b04996>
- Lv JT, Han RX, Huang ZQ, Luo L, Cao D, Zhang SZ (2018) Relationship between molecular components and reducing capacities of humic substances. *ACS Earth Space Chem* 2:330–339. <https://doi.org/10.1021/acsearthspacechem.7b00155>
- Mian MM, Liu GJ, Yousaf B, Fu B, Ullah H, Ali MU, Abbas Q, Munir MAM, Liu RJ (2018) Simultaneous functionalization and magnetization of biochar via NH₃ ambient pyrolysis for efficient removal of Cr(VI). *Chemosphere* 208:712–721. <https://doi.org/10.1016/j.chemosphere.2018.06.021>
- Mu ST, Sun DX, Liu YX, Li J, Zhang HW, Wang J (2022) Ultraviolet-visible and fluorescence spectra indicate the binding and transformation properties of hexavalent chromium in DOM solution. *J Environ Chem Eng* 10:107158. <https://doi.org/10.1016/j.jece.2022.107158>
- Murphy KR, Stedmon CA, Graeber D, Bro R (2013) Fluorescence spectroscopy and multi-way techniques. *PARAFAC Anal Methods* 5:6557–6566. <https://doi.org/10.1039/C3AY41160E>
- Patel KF, Tejnecký V, Ohno T, Bailey VL, Sleighter RL, Hatcher PG (2021) Reactive oxygen species alter chemical composition and adsorptive fractionation of soil-derived organic matter. *Geoderma* 384:114805. <https://doi.org/10.1016/j.geoderma.2020.114805>
- Phillips SM, Smith GD (2015) Light absorption by charge transfer complexes in brown carbon aerosols. *Environ Sci Technol Lett* 1:382–386. <https://doi.org/10.1021/ez500263j>
- Remke SC, Bürgin TH, Ludvíková L, Heger D, Wenger OS, von Gunten U, Canonica S (2022) Photochemical oxidation of phenols and anilines mediated by phenoxyl radicals in aqueous solution. *Water Res* 213:118095. <https://doi.org/10.1016/j.watres.2022.118095>
- Remke SC, Houska J, von Gunten U, Canonica S (2023) Impact of chlorination and ozonation of dissolved organic matter on its photo-induced production of long-lived photooxidants and excited triplet states. *Water Res* 239:119921. <https://doi.org/10.1016/j.watres.2023.119921>
- Ruan XX, Sun YQ, Du WM, Tang YY, Liu Q, Zhang ZY, Doherty W, Frost RL, Qian GR, Tsang DCW (2019) Formation, characteristics, and applications of environmentally persistent free radicals in biochars: a review. *Bioresour Technol* 281:457–468. <https://doi.org/10.1016/j.biortech.2019.02.105>
- Song JZ, Li MJ, Jiang B, Wei S, Fan XJ, Peng PA (2018) Molecular characterization of water-soluble humic like substances in smoke particles emitted from combustion of biomass materials and coal using ultrahigh-resolution electrospray ionization Fourier transform ion cyclotron resonance mass spectrometry. *Environ Sci Technol* 52:2575–2585. <https://doi.org/10.1021/acs.est.7b06126>
- Spencer RGM, Guo WD, Raymond PA, Dittmar T, Hood E, Fellman J, Stubbins A (2014) Source and biolability of ancient dissolved organic matter in glacier and lake ecosystems on the Tibetan Plateau. *Geochim Cosmochim Acta* 142:64–74. <https://doi.org/10.1016/j.gca.2014.08.006>
- Stedmon CA, Markager S (2005) Resolving the variability in dissolved organic matter fluorescence in a temperate estuary and its catchment using PARAFAC analysis. *Limnol Oceanogr* 50(2):686–697. <https://doi.org/10.4319/lo.2005.50.2.0686>
- Tang J, Li J, Su T, Han Y, Mo YZ, Jiang HX, Cui M, Jiang B, Chen YJ, Tang JH, Song JZ, Peng PA, Zhang G (2020) Molecular compositions and optical properties of dissolved brown carbon in biomass burning, coal combustion, and vehicle emission aerosols illuminated by excitation-emission matrix spectroscopy and Fourier transform ion cyclotron resonance mass spectrometry analysis. *Atmos Chem Phys* 20:2513–2532. <https://doi.org/10.5194/acp-20-2513-2020>
- Tang J, Wang JQ, Zhong GC, Jiang HX, Mo YZ, Zhang BL, Geng XF, Chen YJ, Tang JH, Tian CG, Bualert S, Li J, Zhang G (2021) Measurement report: Long-emission-wavelength chromophores dominate the light absorption of brown carbon in aerosols over Bangkok: impact from biomass burning. *Atmos Chem Phys* 21:11337–11352. <https://doi.org/10.5194/acp-21-11337-2021>
- Vejerano E, Lomnicki S, Dellinger B (2011) Formation and stabilization of combustion-generated environmentally persistent free radicals on an Fe(III)₂O₃/silica surface. *Environ Sci Technol* 45:589–594. <https://doi.org/10.1021/es102841s>
- Waggoner DC, Hatcher PG (2017) Hydroxyl radical alteration of HPLC fractionated lignin: formation of new compounds from terrestrial organic matter. *Org Geochem* 113:315–325. <https://doi.org/10.1016/j.orggeochem.2017.07.011>
- Waggoner DC, Chen HM, Willoughby AS, Hatcher PG (2015) Formation of black carbon-like and alicyclic aliphatic compounds by hydroxyl radical initiated degradation of lignin. *Org Geochem* 82:69–76. <https://doi.org/10.1016/j.orggeochem.2015.02.007>
- Wang Y, Zhang ZY, Han LF, Sun K, Jin J, Yang Y, Yang Y, Hao ZN, Liu JF, Xing BS (2019) Preferential molecular fractionation of dissolved organic matter by iron minerals with different oxidation states. *Chem Geol* 520:69–76. <https://doi.org/10.1016/j.chemgeo.2019.05.003>
- Wang XD, Xu J, Liu J, Liu J, Xia F, Wang CC, Dahlgren RA, Liu W (2020) Mechanism of Cr(VI) removal by magnetic greigite/biochar composites. *Sci Total Environ* 700:134414. <https://doi.org/10.1016/j.scitotenv.2019.134414>
- Westerhoff P, Aiken G, Amy G, Debroux J (1999) Relationships between the structure of natural organic matter and its reactivity towards molecular

- ozone and hydroxyl radicals. *Water Res* 33:2265–2276. [https://doi.org/10.1016/S0043-1354\(98\)00447-3](https://doi.org/10.1016/S0043-1354(98)00447-3)
- Worms IAM, Chmiel HE, Traber J, Tofield-Pasche N, Slaveykova VI (2019) Dissolved organic matter and associated trace metal dynamics from river to lake, under ice-covered and ice-free conditions. *Environ Sci Technol* 53(24):14134–14143. <https://doi.org/10.1021/acs.est.9b02184>
- Xu XY, Huang H, Zhang Y, Xu ZB, Cao XD (2019) Biochar as both electron donor and electron shuttle for the reduction transformation of Cr(VI) during its sorption. *Environ Pollut* 244:423–430. <https://doi.org/10.1016/j.envpol.2018.10.068>
- Xu J, Dai YC, Shi YF, Zhao S, Tian HX, Zhu KC, Jia HZ (2020a) Mechanism of Cr(VI) reduction by humin: role of environmentally persistent free radicals and reactive oxygen species. *Sci Total Environ* 725:138413. <https://doi.org/10.1016/j.scitotenv.2020.138413>
- Xu ZB, Xu XY, Tsang DCW, Yang F, Zhao L, Qiu H, Cao XD (2020b) Participation of soil active components in the reduction of Cr(VI) by biochar: differing effects of iron mineral alone and its combination with organic acid. *J Hazard Mater* 384:121455. <https://doi.org/10.1016/j.jhazmat.2019.121455>
- Xu Q, Li G, Fang L, Sun Q, Han RX, Zhu Z, Zhu YG (2023) Enhanced formation of 6PPD-Q during the aging of tire wear particles in anaerobic flooded soils: the role of iron reduction and environmentally persistent free radicals. *Environ Sci Technol* 57:5978–5987. <https://doi.org/10.1021/acs.est.2c08672>
- Yang J, Pan B, Li H, Liao SH, Zhang D, Wu M, Xing BS (2016a) Degradation of p-nitrophenol on biochars: role of persistent free radicals. *Environ Sci Technol* 50:694–700. <https://doi.org/10.1021/acs.est.5b04042>
- Yang JP, Zhao YC, Ma SM, Zhu BB, Zhang JY, Zheng CG (2016b) Mercury removal by magnetic biochar derived from simultaneous activation and magnetization of sawdust. *Environ Sci Technol* 50:12040–12047. <https://doi.org/10.1021/acs.est.6b03743>
- Yang ZH, Zhang XM, Jiang Z, Li Q, Huang PC, Zheng CJ, Liao Q, Yang WC (2021) Reductive materials for remediation of hexavalent chromium contaminated soil—a review. *Sci Total Environ* 773:145654. <https://doi.org/10.1016/j.scitotenv.2021.145654>
- Yuan Y, Bolan N, Prévosteau A, Vithanage M, Biswas JK, Ok YS, Wang HL (2017) Applications of biochar in redox-mediated reactions. *Bioresour Technol* 246:271–281. <https://doi.org/10.1016/j.biortech.2017.06.154>
- Zeng Q, Wang X, Liu XL, Huang LQ, Hu JL, Chu R, Tolic N, Dong HL (2020) Mutual interactions between reduced Fe-bearing clay minerals and humic acids under dark, oxygenated conditions: hydroxyl radical generation and humic acid transformation. *Environ Sci Technol* 54(23):15013–15023. <https://doi.org/10.1021/acs.est.0c04463>
- Zeng Y, Fang GD, Fu QL, Dionysiou DD, Wang XL, Gao J, Zhou DM, Wang YJ (2021) Photochemical characterization of paddy water during rice cultivation: formation of reactive intermediates for As(III) oxidation. *Water Res* 206:117721. <https://doi.org/10.1016/j.watres.2021.117721>
- Zhang BP, Zhou SF, Zhou LH, Wen JL, Yuan Y (2019) Pyrolysis temperature-dependent electron transfer capacities of dissolved organic matters derived from wheat straw biochar. *Sci Total Environ* 696:133895. <https://doi.org/10.1016/j.scitotenv.2019.133895>
- Zhang KK, Khan A, Sun P, Zhang Y, Kamal A, Zhang YR (2020) Simultaneous reduction of Cr(VI) and oxidization of organic pollutants by rice husk derived biochar and the interactive influences of coexisting Cr(VI). *Sci Total Environ* 706:135763. <https://doi.org/10.1016/j.scitotenv.2019.135763>
- Zhang K, Gao J, Men DP, Zhao XY, Wu SS (2021) Insight into the heavy metal binding properties of dissolved organic matter in mine water affected by water-rock interaction of coal seam goaf. *Chemosphere* 265:129134. <https://doi.org/10.1016/j.chemosphere.2020.129134>
- Zhong DL, Zhang YR, Wang LL, Chen J, Jiang Y, Tsang DCW, Zhao ZZ, Ren SP, Liu ZH, Crittenden JC (2018) Mechanistic insights into adsorption and reduction of hexavalent chromium from water using magnetic biochar composite: key roles of Fe₃O₄ and persistent free radicals. *Environ Pollut* 243:1302–1309. <https://doi.org/10.1016/j.envpol.2018.08.093>
- Zhu SS, Huang XC, Yang XB, Peng P, Li ZP, Jin C (2020) Enhanced transformation of Cr(VI) by heterocyclic-N within nitrogen-doped biochar: impact of surface modulatory persistent free radicals (PFRs). *Environ Sci Technol* 54:8123–8132. <https://doi.org/10.1021/acs.est.0c02713>
- Zhu YP, Xie QR, Zhu RL, Lv Y, Xi YF, Zhu JX, Fan J (2022) Hydrothermal carbons/ferrhydrite heterogeneous Fenton catalysts with low H₂O₂ consumption and the effect of graphitization degrees. *Chemosphere* 287:131933. <https://doi.org/10.1016/j.chemosphere.2021.131933>
- Zhuo CY, Zhang DN, Yang Y, Ran Y, Zhang XY, Mao JD (2019) Effects of compositions, chemical structures, and microporosity of sedimentary organic matter on degradation of benzo(a)pyrene by hydrogen peroxide. *Water Res* 159:414. <https://doi.org/10.1016/j.watres.2019.05.041>